Temperature field acquisition by planar laser induced fluorescence using the two-color/two-dye technique for liquid flows in a millimetric zigzag channel

Hanbin Shi, Nathalie Di Miceli Raimondi, Emmanuel Cid, Michel Cabassud, Christophe Gourdon

Temperature field acquisition by a Planar Laser Induced Fluorescence using the two-color/two-dye technique for liquid flows in a millimetric zigzag channel

Hanbin SHI[a], Nathalie DI MICELI RAIMONDI[a,*], Emmanuel CID[a], Michel CABASSUD[a], Christophe GOURDON[a]

[a] *Laboratoire de Génie Chimique, Université de Toulouse, CNRS, INPT, UPS, Toulouse, France*

[*] *E-mail address: nathalie.raimondi@iut-tlse3.fr*

Abstract

The acquisition of local temperature fields in compact reactors is essential to understand the heat transfer mechanisms in these often-complex geometry devices, and to detect the presence of any dead zones where hot or cold spots can appear during implementation of reactions. In this work, thermometry by PLIF method (Planar Laser Induced Fluorescence) is implemented in a square millimetric zigzag channel of 4 mm depth. The two-color/two-dye method is used. The advantages of this technique are that it is non-intrusive and it presents a very good spatial and temporal resolution. The method is first calibrated capturing temperature fields in flowing water at constant temperature. The sensitivity of the implemented method is good, equals to 3.3%.C^{-1} in terms of fluorescence signal ratio. Uncertainty of 0.6% of the measured temperature is due to the noise of the acquired images, and the global uncertainty of the measurement is estimated to be lower than 3% in the temperature range of 17-60°C. The PLIF technique is then applied during heat transfer to obtain temperature fields at different positions and heights in the channel. The average temperatures measured from the local temperature fields are close to the temperature profiles calculated with a 1D heat transfer model. The obtained results show the potential of the PLIF technique to detect temperature heterogeneities in compact devices for the study and the design of intensified reactors.

Keywords: Local thermometry; Planar Laser Induced Fluorescence; Heat transfer; Microchannel; Compact reactors; Process intensification

1. Introduction

In the past decades, numerous compact reactors have been developed to meet the challenges of process intensification in the chemical industry. As an example, compact heat exchangers reactors present very good thermal performances in terms of heat exchange capacity due to high heat transfer coefficient and very high exchange area compared to reactor volume [1,2]. They are considered as an alternative to batch or fed-batch reactors for the implementation of exothermic and fast reactions that pose safety and product quality concerns. However, manufacturers are still quite rare to have seized the opportunity to integrate these intensified reactors into their production chains. The reasons for such restraints are first of all the equipment and operating protocol changes, in particular related to a transposition from discontinuous to continuous reaction process in innovative devices. The lack of correlations and scale-up laws also slows-down decision-making toward greater use of the devices at industrial scale while performant compact reactors with reasonable capacity are today available (of a few m^3 per day). It is therefore important to obtain models to estimate compact reactors performances in order to be able to

assess the feasibility of a reaction scheme implementation in such devices, to predesign the process and to evaluate its profitability. These models should be established from accurate data depending on the performance to characterize to be reliable enough. In compact heat-exchanger reactors, it is particularly interesting to model global heat exchange capacity and also to study local velocity and temperature fields in order to detect potential dead zones. Such zones can generate hot spots during exothermic reaction processing that promote undesired reactions (by-products production, component decompositions that may cause thermal runaway…).

In order to understand how hydrodynamics and heat transfer are coupled in heat exchangers reactors, the acquisition of local information such as velocity and temperature fields is fundamental. Indeed, it is of great help for process modeling, design optimization and scale-up. Particle Image Velocimetry (PIV) has been widely used in the past decades to obtain accurate velocity fields of fluids in devices and channels with various sizes [3], even at microscale [4]. Techniques for local temperature measurements are available but their performance in terms of accuracy and response time need to be discussed in terms of use in millimetric channels. So, it is required to develop new experimental methods or to adapt existing techniques to characterize heat transfer performance in compact intensified devices.

The present work focuses on the use of an experimental thermometry method based on planar laser induced fluorescence to observe temperature fields in liquids. The method is originally applied to confined liquids that flow in zigzag millimetric square channels. These channels can be used as a basic pattern for compact heat-exchanger reactor design [5,6]. Indeed, curved channels generate secondary flows so-called Dean vortices improving mixing over the channel cross-section and so heat transfer even at low Reynolds number [7–10]. First, the experimental methods available to measure local temperatures are described and discussed regarding their applicability in millimetric channels. Then a detailed focus is made on the optical thermometry technique based on planar laser-induced fluorescence technique. Finally, this method is applied to measure temperature fields in compact heat-exchanger reactor prototypes composed of zigzag channels. The materials used and the calibration protocol are described prior to the presentation of the results.

2. Review of common temperature measurement methods

There are many methods to measure the temperature such as thermoelectric devices, platinum resistance thermometers or optical thermography techniques. The objective of this part is to present briefly these methods and discuss their suitability to compact devices with millimetric channels. Thermocouples are thermoelectric devices commonly used because of their low cost, simplicity, small size and robustness. They have a lot of advantages as well as the speed of response and their large scale of measurements. They are more accurate than resistance temperature devices (RTD) which are also widely used to measure temperature. Moreover RTD are self-heating (the current through the sensor causes some heating) which tends to provide an artificially higher temperature. Both thermocouples and RTD are cheap devices, easy to use but they have a limited spatial resolution, e.g. some zones may be difficult to reach in a fluid flow. In addition, the probes have to be inserted in the fluid to obtain enough accurate results, which can cause disturbances within the flow. Such intrusive techniques are therefore not suitable for local temperature field acquisition and non-intrusive optical techniques should be preferred.

Optical methods based on the use of components with at least one optical property sensitive to temperature can be used. As an example, microencapsulated thermochromic liquid crystal (TLC) can be introduced in a liquid flow to measure its local temperature [11,12]. When they are illuminated, the

intensity of the reflection signal is sensitive to the local temperature. However, this technique is not commonly used as its accuracy is medium due to illuminating light variation, wall reflection and scattering. It requires a very sophisticated calibration protocol to improve the measurement reliability. Moreover, TLCs are particles and their position in a flowing fluid depends on the hydrodynamics: so, temperature fields in dead zones may be difficult to observe.

Infrared thermography (IRT) is a contact-free technique for temperature measurements, based on the emission of thermal radiation of an object which depends on the temperature. In the last decades, IRT has become a powerful means of thermo-dynamic analysis to measure convective heat fluxes as well as to investigate the surface flow field behaviour over complicated body shapes. This technique has been used in microreactors and compact reactors [13–17]. IRT has advantages like high spatial resolutions of surface temperatures and immediate response. However, IRT is limited to outside surfaces, so it is not adapted for local temperature field measurement in fluid flow. Thermal diffusion in the outside surface material and its thermal inertia dramatically affect the method accuracy in particular to observe very little zones and transient effects.

Laser-induced fluorescence (LIF) technique is based on the temperature dependence of fluorescence emission of dyes. Contrary to IRT, it allows to measure directly the local temperature in fluids. LIF technique for fluid temperature measurement is less often used than the other measurement methods because it requires expensive and large equipments (laser, cameras, etc.). However, it is interesting for local temperature measurements because this technique is non-intrusive, presents a very high spatial resolution and provides immediate response which can be adapted to unsteady flows. Planar laser-induced fluorescence (PLIF) is generally implemented, using a laser sheet, in order to obtain 2D temperature fields in the region-of-interest. Different approaches to implement PLIF in liquids have been developed. The simplest technique uses a single dye and a single spectral band to measure the temperature. Nakajima et al. [18] and Lemoine et al. [19] used rhodamine B to measure the temperature in turbulent heat transfer. Sakakibara et al. [20] measured the temperature in thermally stratified pipe flow with the rhodamine B. Coolen et al. [21] performed temperature measurements with the rhodamine B in a natural convection flow. For this technique, the problem is that any disturbance of fluorescence signal can influence the measurement of temperature as the temperature is directly deduced from the fluorescence intensity, for example the temporal variation of laser intensity, the change of dye concentration. The flow itself can influence the fluorescence signal as well, like in multiphase flows, the interfaces of droplets and bubbles can change light propagation. To limit the impact of these disturbances, the ratiometric technique has been developed. In this technique, two detection bands are used and the temperature can be deduced from the ratio of the fluorescence intensity of these two bands. In some studies, one dye with two bands (2c/1d) having different temperature sensibilities are utilized. Bruchhausen et al. [22] studied the one-phase flow by using the two-color/single-dye technique with rhodamine B. Castanet et al. [23] measured the temperature field within the droplets with the same technique using the pyrromethene 597-C8. However, the most popular method is using two dyes with two detection bands, so-called two-color/two-dye (2c/2d) technique. In this approach, normally a temperature-sensitive dye is associated with another little temperature-sensitive dye. Sakakibara and Adrian [24,25] conducted temperature measurements in a stable thermally stratified layer with the couple of dyes Rhodamine B/Rhodamine 110 and then applied this technique to the measurement of temperature field in turbulent Rayleigh-Bénard convection flow. The same couple of dyes was used by Kim et al. for temperature mapping in a 1 mm wide closed heated cuvette [26]. Chaze et al. [27] used the couple of dyes fluorescein disodium/sulforhodamine 640 and obtained single-shot images of the temperature inside droplets. In some other studies, the two dyes with opposite temperature sensibilities are utilized which can obtain higher sensibilities to the temperature. Sutton et al. [28] performed an

improved temperature-sensitive LIF measurement in aqueous fluid flows using the couple of dyes fluorescein disodium/kiton red (also called sulforhodamine B). Shafii et al. [29] reported an in situ whole-field measurements of the temperature field in aqueous ammonium chloride solution during uni-directional solidification using the same couple of dyes.

Finally, it should be noted that few works have used a fluorescence technique in channels of small diameters for temperature measurement. Filevich and Etchenique measured the axial temperature profile in a 0.86 mm diameter circular tube using a rhutenium complex as the fluorescent dye and a high power LED as the excitation source [30]. Pfeiffer and Nagl have reviewed some works where the fluorescence technique has been used to measure the temperature in microfluidic chips [31], not directly in the liquid but by embedding fluorescent particles in a solid matrix coated on the wall of the channel, or by using fluorescent microdroplets within the liquid flow [32]. In the present work, PLIF thermometry with the two-color/two-dye approach is therefore used in an original way for the temperature measurement of liquids in a compact heat exchanger reactor composed of a millimetric zigzag channel. This method is described in detail in the next section.

3. Principle of temperature measurement in liquids based on two dyes PLIF technique

The fluorescence signal dF_λ emitted at a wavelength λ in an elementary volume dV of liquid can be expressed as [33]:

$$dF_\lambda = \eta \frac{\Omega}{4\pi} \varepsilon_0 \phi_\lambda \frac{I_0}{(1+\frac{I_0}{I_{sat}})} C dV \tag{1}$$

where η is the transmission efficiency of the fluorescence light of the detector, Ω is the solid angle of the collection, ε_0 is the molar absorptivity of the fluorescent molecules at the excitation wavelength of the laser beam, ϕ_λ is the fluorescence quantum yield, I_0 is the laser intensity in the volume dV, I_{sat} is the saturation intensity of the fluorescent dye, C is the molar concentration of the dye. In this equation, ε_0, ϕ_λ, I_{sat} are dependent on the temperature. ϕ_λ decreases with the temperature due to collisional quenching while I_{sat} increases with the temperature [27]. However, it has been shown that temperature dependence of fluorescence signal follows rigorously that of molar absorptivity for fluorescein disodium [27] and fluorescein 27 [28] at a given wavelength. Assuming this same behavior for all the dyes, for a homogenous solution (C is constant), the ratio of the fluorescence signal at a temperature T and a reference one T_0 can be expressed as follows:

$$\frac{dF_\lambda(T)}{dF_\lambda(T_0)} = \frac{\varepsilon_0(T)}{\varepsilon_0(T_0)} \tag{2}$$

This expression can be used as far as the laser intensity I_0 is constant. However, using the two-color/two-dye approach allows accounting for possible intensity variation to obtain the following expression, assuming no spectral conflicts between the two dyes used (absorption and emission spectra do not superimpose in the spectral bands λ_1 and λ_2 of observation):

$$\frac{dF_{\lambda1}(T)/dF_{\lambda1}(T_0)}{dF_{\lambda2}(T)/dF_{\lambda2}(T_0)} = \frac{\varepsilon_{0,\text{dye\_1}}(T)/\varepsilon_{0,\text{dye\_1}}(T_0)}{\varepsilon_{0,\text{dye\_2}}(T)/\varepsilon_{0,\text{dye\_2}}(T_0)} \tag{3}$$

The analysis of the spectra of absorption and fluorescence emission of different dyes is necessary for choosing the adequate couple of dyes. First of all, the dyes should display different sensitivities to temperature in terms of emission spectra to avoid that the ratio in Eq. (3) equals one whatever the temperature is. Chaze *et al.* studied the temperature sensitivity of 8 common dyes [33]. Fluorescein

disodium (FL) is chosen as one of the dyes in the present work because of its high sensitivity (fluorescence intensity increases significantly with increasing temperature), independently of wavelength under 580 nm. Sulforhodamine B sodium (SRB or kiton red) is the other dye used in this work which has a negative temperature sensitivity compared to FL. FL and SRB present sensitivity coefficients of $+3.22\%.°C^{-1}$ (at pH = 5.6) and $-2.43\%.°C^{-1}$ respectively [27]. The use of two dyes with opposite temperature sensitivity can improve the accuracy of the measurement as mentioned above. Moreover the absorption and emission spectra of SRB are red-shifted which can reduce the spectra conflicts in the two dyes approach, problem mentioned by Coppeta and Roger [34]. Fluorescein can exist in different protolytic forms depending on the pH of the aqueous solution (cation/neutral form/monoanion/dianion, $pK_a = 2.2, 4.4, 6.7$) that depict different absorption and fluorescence emission spectra [35]. Neutral form presents low absorption intensity in the visible domain. Dianion form is chosen in the present work since it is characterized by narrower absorption and emission spectra compared to the other ionic forms, reducing potential spectra conflicts. Therefore, dye solutions are prepared at a pH of 10 using a carbonate buffer. SRB has been chosen instead of sulforhodamine 640 (SR640) since SR640 is subject to photodegradation in the presence of FL, especially above 60 °C, and because the emission temperature sensitivity of FL/SRB is higher than that of FL/SR640 [27,33]. PLIF thermometry using FL/SRB couple has already been applied [28,29]. However, unlike FL and SR640, SRB fluorescence signal intensity is also sensitive to laser irradiance I_0: Chaze *et al.* suggested that FL/SRB couple should be only used in uniformly illuminated region [33]. This can be reasonably assumed in millimetric channels where the liquid thickness crossed by the laser beam is low (from 2 to 5.7 mm in the present work).

Absorption and emission spectra for dianionic form of FL at room temperature are available in the literature [33,36], as represented in Fig. 1. A laser that emits at 532 nm has been used according to that used in similar studies [27,28]. Therefore, as described afterwards, the concentration of FL in the experiment is much higher than that of SRB because of its relatively low intensity of absorption at such wavelength. The two detection bands used in the experiment are shown in Fig. 1:

- Band 1 [543-549 nm]: FL has a predominant contribution in this band. SRB has some contribution. Moreover, in this spectral band, it appears that SRB may reabsorb part of the emission signal of FL. However, as concentration of SRB is very low compared to that of FL, these spectral conflicts are neglected.
- Band 2 [>633 nm]: The emission of SRB is predominant. The emission of FL is not totally negligible and its contribution depends on the respective concentration of the dyes. However, the effect of this spectral conflict on the different measurements can be neglected because the same dye solution is used during calibration and all experiments. Therefore, the ratio of FL and SRB concentrations is constant and uniform throughout the present study.

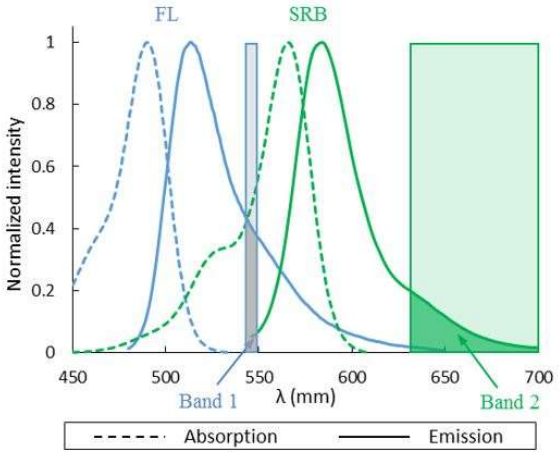

Fig. 1. Detection bands used for the PLIF technique with the dye couple FL/SRB. Laser emission wavelength is 532 nm

Neglecting the emission and absorption by SRB in band 1 and the emission of FL in band 2, the ratio R between the fluorescence signals detected on the two bands can be determined:

$$R = \frac{dF_{\lambda 1}(T)}{dF_{\lambda 2}(T)} \tag{4}$$

A measurement at the reference temperature T_0 allows determining the ratio R_0:

$$R_0 = \frac{dF_{\lambda 1}(T_0)}{dF_{\lambda 2}(T_0)} \tag{5}$$

Finally, normalized fluorescence ratio at one temperature T can be expressed as follows using Eq. (3):

$$R_{normalized} = \frac{R}{R_0} = \frac{\varepsilon_{0,FL}(T)}{\varepsilon_{0,SRB}(T)} \frac{\varepsilon_{0,SRB}(T_0)}{\varepsilon_{0,FL}(T_0)} = \mathrm{f}(T) \tag{6}$$

where f is the calibration function obtained from a prior calibration of the method that will be described afterwards. The temperature can finally be determined :

$$T = f^{-1}\left(\frac{R}{R_0}\right) \tag{7}$$

4. Materials

4.1. Chemicals

An aqueous solution of dyes is prepared using the following chemicals: fluorescein sodium technical (FL, VWR International SAS, CAS: 518-47-8); sulforhodamine B sodium salt (SRB, Alfa Aesar, CAS: 3520-42-1); carbonate buffer (pH=10, Acros Organics BVBA). A solution of 5 µmol.L^{-1} of SRB and 0.2 mmol.L^{-1} of FL in 800 mL of demineralized water and 200 mL of carbonate buffer is prepared. The concentration of FL have been chosen in agreement with that used by Chaze et al. who used this dye for temperature field measurement inside droplets impinging on a hot solid surface [27]. In their study, they used similar optical materials than those used in the present study (a pulsed Nd:YAG laser at 532 nm

and CCD cameras). The high concentration of FL compared to SRB is due to the low absorption of FL at 532 nm, in order to obtain comparable fluorescence emission intensity on both images.

4.2. Experimental prototype

A heat exchanger reactor prototype is studied in order to measure the temperature field within the process fluid during heat transfer operation, without reaction. The prototype consists of two plates where millimetric channels are engraved, named "process channel" and "utility channel" as illustrated in Fig. 2. The plates are made of PolyMethylMethAcrylate (PMMA) 10 mm thick. This hard-polymeric material has been chosen because it is cheap and can be easily engraved by milling. It is transparent which is convenient for flow observation and also necessary for the temperature field measurement. Moreover, its thermal conductivity is very low which allows to limit heat loss (k = 0.19 W $m^{-1}K^{-1}$, e/k = 0.05 $m^2K\ W^{-1}$). The two channels are separated by an aluminum wall (Fig. 2). The PMMA plates are pasted to the aluminum plate using double-sided adhesives cut to fit the channel designs. The aluminum plate is 1 mm thick with a high thermal conductivity (k = 237 W $m^{-1}K^{-1}$) and its thermal resistance is very low ($e/k = 4.2 \times 10^{-6}\ m^2K\ W^{-1}$). Its surface has been anodized to obtain a non-metallic black color which can allow the safe use of the laser for the temperature field measurement by PLIF.

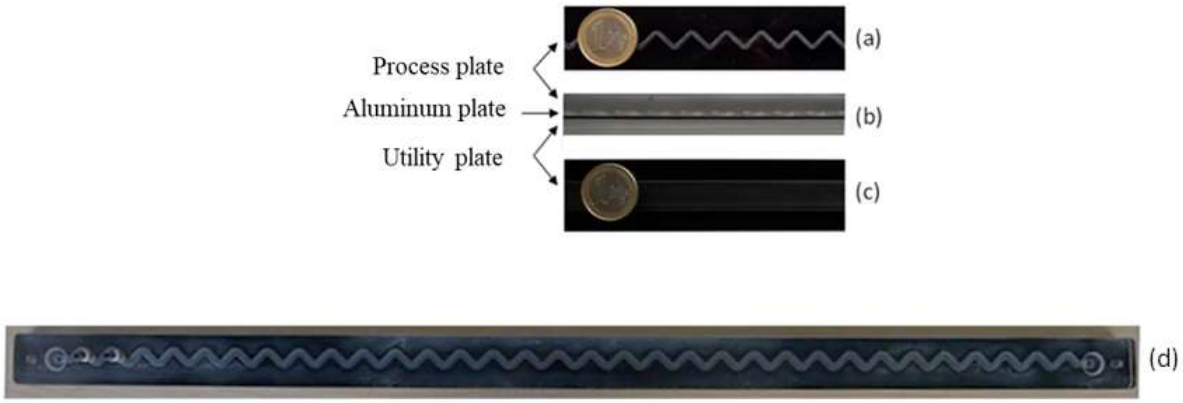

Fig. 2. Heat-exchanger prototype composed of a PMMA plates with a square zigzag channel engraved (a) and a rectangular straight channel engraved (c) separated by an aluminum wall (middle in (b)). Top view of the prototype (length = 65 cm, width = 3 cm) (d)

In this work, temperature measurement in the millimetric zigzag channel is of interest as it is a geometry pattern used to build compact heat-exchanger reactors of flow capacity of 1 to 50 $L.h^{-1}$. Such devices made of silicon carbide or stainless steel have been successfully used to carry out highly exothermic reactions [5,6,37]. The zigzag channel consists of periodic straight sections and bends, as shown in Fig. 3. The channel presents a square cross-section of hydraulic diameter d_h = 4 mm. The mean curvature radius of the bends R_c is 3 mm, the straight section length L_s is 7 mm and the angle θ between two straight sections is 90°. Heat transfer in such a geometry pattern has been previously studied based on CFD simulations [10]. The utility channel presents a rectangular cross-section of 12 mm width and 6 mm depth (hydraulic diameter d_h = 8 mm). It is large enough to sufficiently cover the zigzag process channel. The utility and process channels are face to face and centered in the PMMA plates. The geometry parameters of the zigzag process channel and the straight utility channel are presented in Table 1.

Table 1. Geometry parameters of the zigzag process channel and the straight utility channel (S is the cross-sectional area and L is the total developed length of the channel)

	S (mm^2)	d_h (mm)	R_c (mm)	θ (°)	L_s (mm)	L (mm)
Process channel	4×4	4	3	90	7	747
Utility channel	12×6	8	-	-	-	588

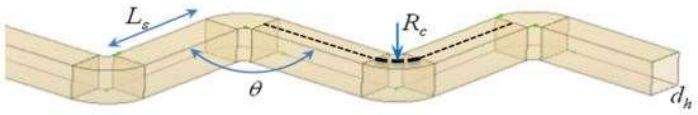

Fig. 3. Schematic of the zigzag channel

4.3 Experimental setup

The experimental setup is presented in Fig. 4. The process channel is connected to a gear pump (0 - 100 L h^{-1}) and the utility channel is connected to a centrifugal pump (0 - 1000 L h^{-1}). Mass flowrates are measured. The process fluid (fluorescent aqueous solution) is heated by a thermostatic bath through a heat exchanger before entering the prototype. It is then cooled in the heat exchanger prototype under study by water circulating in the utility channel. The two fluids circulate co-currently. Four thermocouples are used to measure the inlet and outlet temperatures of the two channels. Temperatures are recorded by an acquisition system based on a LabVIEW software (National Instruments, US) which can also control the gear pump.

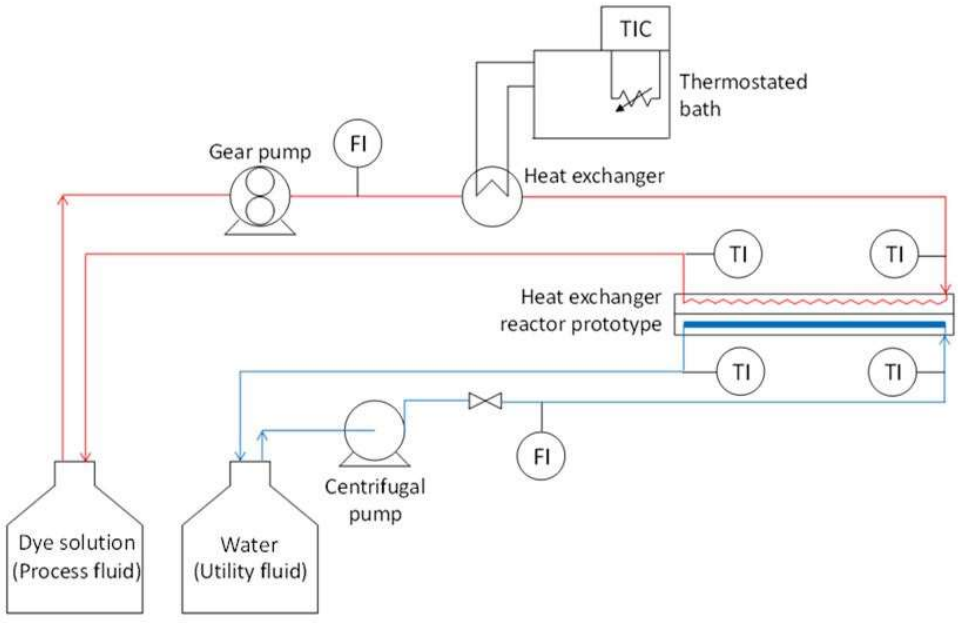

Fig. 4. Pilot plant for the heat transfer study of a heat exchanger reactor prototype

A pulsed Nd:YAG laser at 532 nm (Litron Lasers, Nano L 120-20 PIV, pulse energy E = 63 mJ, pulse duration dt = 4 ns) is used in this work. The thickness of the laser beam is about 500 µm and its width is 12 cm. The repetition rate of the pulsed laser is 10 Hz. The fluorescence is detected by two CCD cameras (Lavision Imager Intense, 1376x1040 pixels, 12 bits) which are placed above the prototype and synchronized with the laser. The field of view (FOV) is limited to 13 mm wide and 7 mm high, illuminated by the central spatial uniform part of the laser beam. The global laser configuration allows to work in a partially saturated fluorescence regime (I_0/I_{sat} = 2.2), adapted for the two-color/two-dye approach and the couple of dyes chosen as far as the observed zone is uniformly illuminated [33]. This assumption is reasonable in the present study as the FOV is very small. The two cameras are equipped with two different interference filters to obtain the fluorescence signals emitted at the two bands of interest, as shown in Fig. 5. The optical detection system is based on a binocular microscope (Leica, M651) with an objective lens which can detect the fluorescence signal. The two cameras are supported by two tubes over the objective lens. The fluorescence signals detected by the cameras are registered computationally.

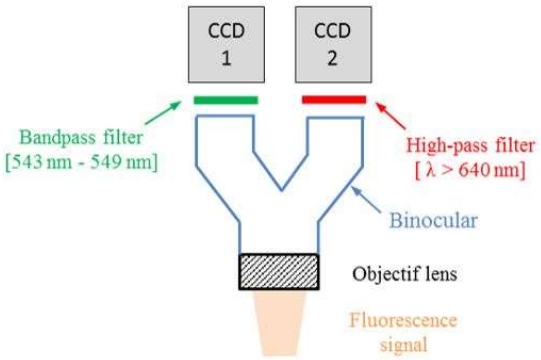

Fig. 5. Optical detection system

The optical system is schematized in Fig. 6. For safety reasons due to laser use, an optical barrier consisting of a black wall is placed after the prototype, at the same level as the zigzag channel in the process plate. The height of the prototype and its transverse position can be adjusted during the experiment while the laser beam and detection system are fixed. With the moving system, the fluorescence signal at different longitudinal positions and different height levels inside the zigzag

channel can be detected. With this optical system, the observed plane is parallel to the top face of the prototype.

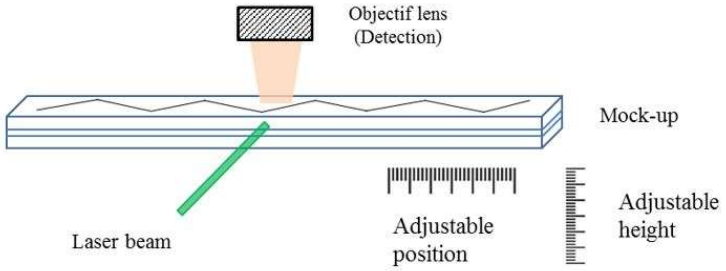

Fig. 6. Optical system for the visualization of fluorescence emission in the zigzag channel

5. Method

5.1 Temperature calibration

Based on the ratio normalization (Eq. (6)) and the low variations (few millimeters) of the optical paths due to the zigzag geometry and the varying depth of the investigated planes, it is assumed that the temperature calibration can be done at one single plane of the studied millimetric channel and be directly applied to the other planes studied afterwards. It avoids the repeating work of temperature calibration at each observed plane. The normalized method can also get rid of potential disturbance effects on the fluorescence signal such as prototype surface defaults, optical reflection at different locations in the channels, etc. The calibration is carried out near the entrance of the zigzag channel, 0.01 m after the channel inlet (channel total length is around 0.75 m). The zone observed is in the middle of the channel (2 mm from the below edge). The flowrate of the fluorescent solution is 4 $kg.h^{-1}$ with no fluid introduced in the utility channel. The inlet and outlet temperatures of the process fluid are measured by thermocouples. During the experiment, the maximum difference between inlet and outlet temperatures is 0.5 °C, therefore the temperature of the zone observed can be considered as the inlet temperature. For the calibration protocol, the fluorescent solution enters the process channel at a temperature ranging from 17 °C to 60 °C (in Table 2), where 24.9 °C is taken as the reference temperature. For each temperature, 100 fluorescence images are taken and registered once thermal equilibrium is reached.

Table 2. Inlet temperatures of fluorescent solution for the calibration protocol (measured by a thermocouple)

$T_{p,in}$ (°C)	17.5	24.9	30.3	36.7	42.7	49.5	52.5	55.9	58.8

5.2 Temperature measurement with heat transfer

During the heat transfer experiments, the fluorescent solution is heated at about 60 °C before entering the process channel. Two flowrates are studied, corresponding to Reynolds number of 503 and 695. The range of *Re* investigated corresponds to laminar flow conditions in millimetric wavy channels [38]. Local temperature heterogeneities are more likely to be observed in this regime. In the utility channel, water at ambient temperature is introduced with a flowrate of 300 $kg.h^{-1}$. Measurements at three longitudinal positions of the zigzag channel are carried out. For each position, images corresponding to

the fluorescence emission are taken at different heights in the channel. All the planes studied (18 in total) are presented in Table 3. For all the measurements, 500 images are taken and registered once heat transfer equilibrium is reached in order to calculate the average fluorescence ratio *R*.

Table 3. Planes investigated for temperature field measurements by PLIF during heat transfer (plane heights are relative to the bottom edge of the channel, in contact with the aluminium wall). Total channel length is 0.75 m

Low plane height	1 mm					
Medium plane height	2 mm					
High plane height	3 mm					
Re	503			695		
Length (m)	0.034	0.069	0.138	0.045	0.092	0.175

To obtain R_0, fluorescence emission at all the planes measured at the reference temperature is also measured. 100 images are registered with just passing the fluorescent solution in the zigzag channel with an inlet temperature of 24.9 °C (without heat transfer).

5.3 Image processing

5.3.1 Image registration between the two cameras

Two images observed simultaneously by the two cameras in the zigzag channel are shown in Fig. 7. It can be seen that the zone observed by the two cameras is not the same, which is due to the slight angular offset of the two optical axes of the binocular microscope which slightly deviate the light trajectory. Therefore, a computational method is first implemented to superimpose the two images (by translation and rotation) to obtain a common observation area (code developed and computed in Matlab). A matrix is obtained by calculating the affine transform function between these two images which uses the normalized cross-correlation to adjust each pair of control points of the two images. The effects of the image vignetting and the background noise to the grey scale of the image are considered, since the zone observed by the two cameras is different. With this matrix, the fluorescence signal ratio *R* (in terms of grey level ratio) between the two cameras at each corresponding pixel can be calculated.

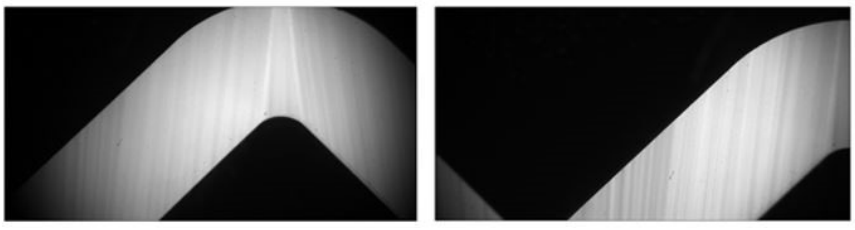

Fig. 7. Fluorescence images simultaneously observed by the two cameras (channel width = 4 mm)

5.3.2 Image registration between an experiment and that at the reference temperature

In the experiment, as the prototype moves slightly with time probably due to bench vibration or thermal dilatation, the zone observed moves a little actually. Thus, another image registration is needed as the fluorescence signal ratio will be normalized with that at the reference temperature (24.9 °C). For a given plane, the zone observed for each experiment (calibration or heat transfer) are repositioned to match the FOV observed at the reference temperature (24.9 °C) by another matrix transform which is obtained by calculating the affine transform functions between the image taken at the reference temperature and that taken at the other temperatures for temperature calibration and heat transfer experiments. With this matrix (different for each case), the fluorescence signal ratio can then be normalized to that at the reference temperature.

6. Results

6.1 Temperature calibration

6.1.1 Calibration equation

The fluorescence ratio R is calculated by dividing the grey level of the two images taken by the two cameras for each corresponding pixel, averaged over the 100 images registered. This is done for all the pixels of the common zone, and for all the calibration experiments at different temperatures. The ratio R is normalized to that obtained at the reference temperature R_0 (24.9 C°), averaged over the 100 images registered as well. A calibration equation is obtained with an exponential regression of the normalized ratio as a function of the temperature in °C:

$$R_{normalized} = \frac{R}{R_0} = \mathrm{f}(T) = \mathrm{e}^{s\cdot(T-T_0)} \tag{8}$$

The coefficient s obtained corresponds to the sensitivity of the measurement to the temperature and equals 3.26%.C^{-1} in the present study. This value shows the good sensitivity of the method. As an example, the calibration curve at the pixel (1000,500) is presented in Fig. 8. It can be seen that the calibration equation fits well with the experimental data. Eq (8) is used for the calculation of all the local temperature measurement at the different planes studied. Fig. 8 also illustrates the uncertainty on s in the determination of the calibration equation from the experimental data. Based on the curves obtained for different pixels, this uncertainty can be reasonably estimated at 0.15%.C^{-1}. The impact of this uncertainty on the global temperature measurement will be discussed in the next section.

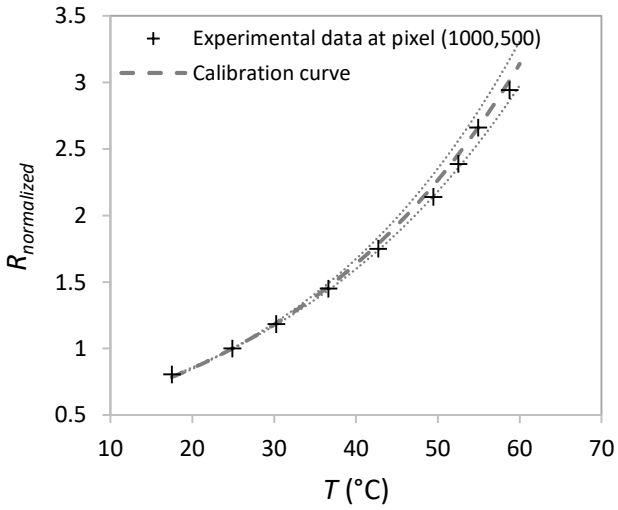

Fig. 8. $R_{normalized}$ vs Temperature measured at a given pixel and calibration curve in dashed line (s = 3.26%.C^{-1}). Dotted lines illustrate the effect of uncertainties on s ($s \pm 0.15\%.C^{-1}$).

6.1.2 Calibration verification and estimation of the uncertainties

A temperature measurement at a high plane (3 mm) between the 5th and the 6th bends (0.059 m from the entrance) is carried out with only introducing the fluorescent solution in the zigzag channel at three temperatures measured by a thermocouple (without heat transfer): 24.9 °C, 36.4°C and 49.2 °C. 100 images of fluorescence signal are registered once steady state is reached. The average fluorescence signal ratio R for the three temperatures is calculated. R at 36.4°C and 49.2 °C is normalized with that obtained at 24.9 °C (the reference temperature). Then, the temperature fields at these two temperatures are deduced using the calibration equation, as shown in Fig. 9. As expected, the temperature field of the zone observed is fairly homogeneous for these two temperatures. The mean temperatures calculated from these two fields are 37.0 °C and 50.1 °C with standard deviations of 0.2°C and 0.3°C respectively, corresponding to a relative standard deviation of 0.6%. The differences between the temperature measured by LIF technique and measured by the thermocouple (at the inlet) are 0.6°C for 36.4°C and 0.9°C for 49.2 °C, showing a difference under 2% of the temperature measured despite the calibration has been realized in another plane (length and height) of the zigzag channel.

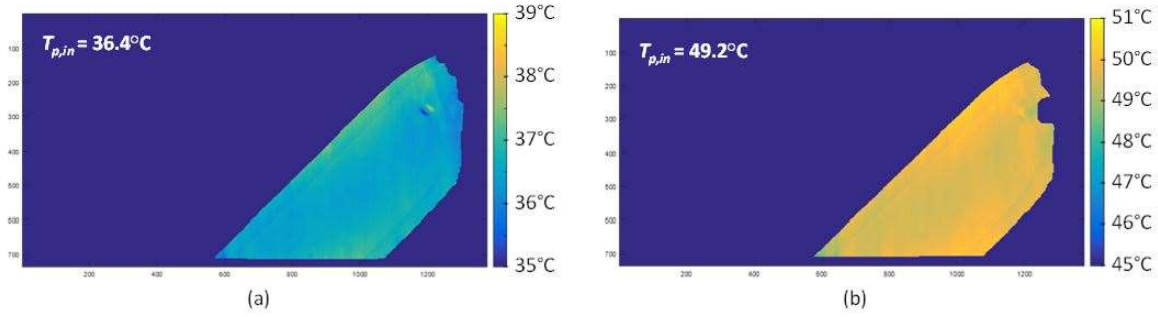

Fig. 9. Average temperature fields at the high plane at 0.059 m from the fluid entrance in the zigzag channel with an inlet temperature of (a) 36.4°C and (b) 49.2 °C (measured by a thermocouple). The fluid flows towards the left. The x- and y-axes correspond to the pixel indices.

In order to have a more accurate interpretation of the results, measurement uncertainty ΔT are estimated. Eq. (8) can be rewritten in terms of Eq. (9) showing that the main sources of uncertainties are the noise of the acquired images $\Delta\eta_R$ (with $\eta_R = \ln(R/R_0)$), the uncertainty due to the determination of the calibration curve ($\Delta s = 0.15\%.°C^{-1}$) and finally the uncertainty of the reference temperature provided by a thermocouple ($\Delta T_0 = 0.3°C$).

$$T = T_0 + \frac{\eta_R}{s} \tag{9}$$

The uncertainty due to noise is estimated using the experiments at constant temperature, where the heterogeneity in the temperature field measured does not depend on the reference temperature and the sensitivity coefficient. Therefore, it is considered that ($\Delta\eta_R$ / η_R) equals the measured relative standard deviation on temperatures, 0.6%. The propagation of the uncertainties can be written as follows [39]:

$$\Delta T = \sqrt{\left(\frac{\partial T}{\partial T_0}\Delta T_0\right)^2 + \left(\frac{\partial T}{\partial s}\Delta s\right)^2 + \left(\frac{\partial T}{\partial \eta_R}\Delta \eta_R\right)^2} = \sqrt{{\Delta T_0}^2 + \left(\frac{\eta_R}{s^2}\Delta s\right)^2 + \left(\frac{\Delta \eta_R}{s}\right)^2} \tag{10}$$

In the temperature range considered, from 17°C to 60°C, ΔT varies between 0.31°C (at the reference temperature) and 1.7°C, giving a relative uncertainty up to 2.8%. In particular, for the experiments at 36.4°C and 49.2 °C, the relative differences measured with the thermocouple (0.6°C and 0.9°C respectively) are consistent with the uncertainty estimation that gives 0.61°C and 1.2°C respectively.

6.2 Temperature measurement with heat transfer

The fluorescence ratio R for all the planes measured during the heat transfer experiments are calculated and normalized to that at the reference temperature obtained without heat transfer (average of 100 images). Two instantaneous temperature fields obtained at the low plane at 0.034 m from the entrance of the zigzag channel for Re = 503 are presented in Fig. 10 (a) and (b). The acquisition time between these two temperature fields is 0.5 s. It can be observed that the cold zones move between the two instantaneous temperature fields, indicating the flow is not in steady laminar regime. Indeed, during the acquisition the stream movement of flow was already observed. The temperature field averaged over 500 images at the low plane for this position is presented in Fig. 10 (c). The mean temperature of the zone observed is 51.8 °C with a standard deviation of 1.2 °C. As expected, standard deviation is here higher than without heat transfer where the fluid temperature is supposed to be roughly constant over the zone observed.

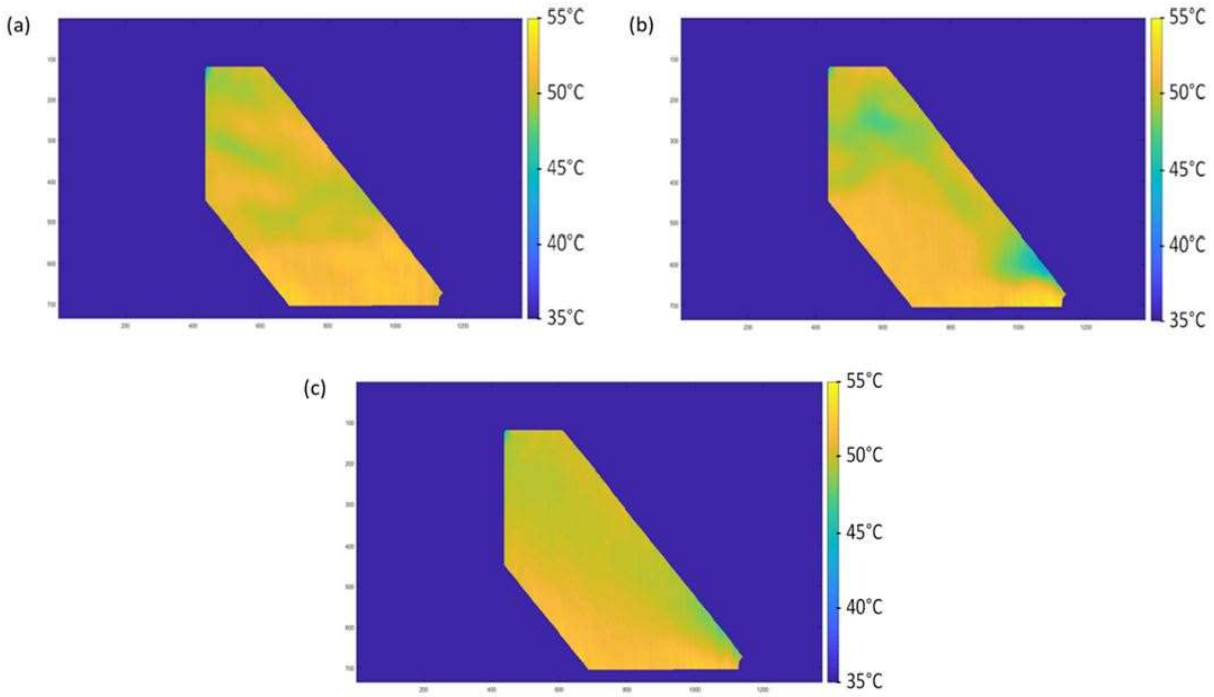

Fig. 10. Instantaneous (a and b) and average (c) temperature fields obtained at the low plane at 0.034 m from the fluid entrance in the zigzag channel, *Re* = 503. The fluid flows towards the left. The x- and y-axes correspond to the pixel indices.

The temperature fields for the all planes studied are obtained and the mean temperature ($T_{p,PLIF}$) is calculated as well, presented in Table 4 for the two flowrate conditions. The inlet and outlet temperatures of the process fluid in the zigzag channel ($T_{p,in}$, $T_{p,out}$) and of the utility fluid in the straight channel ($T_{u,in}$) for all the experiments are also presented in this table. They correspond to mean values between the three experiments carried out (high, medium and low planes). As an example, for the experiment at the length x = 0.138 m in the zigzag channel with *Re* = 503, the mean inlet temperatures measured by the thermocouples of the process fluid and the utility fluid are 56.9 °C and 21.1 °C, the mean outlet temperatures are 29.6 °C and 21.8 °C. The mean temperatures of the process fluid at the three planes (high, medium and low) measured by PLIF are 49.4 °C, 46.6 °C and 47.0 °C. As expected, they are between the inlet and the outlet temperature. It can be observed that the mean temperature globally decreases with the x-position. This is expected, because the process fluid enters hot and is cooled by the utility fluid. However, at a specific height, notably for the high plane, the temperature measured does not always decrease with the x-position. In addition, among the three planes at one length, the low plane is the closest to the cold fluid but is not always the coldest measured. This can be explained by the particular hydrodynamics in wavy channels at the studied *Re*. Indeed, fluid motion tangential to the main direction of the flow appears since channel curvatures generates so-called Dean vortices, unlikely to fluid flow in laminar flow regime in straight channels where streamlines strictly follow the main fluid direction. This particular hydrodynamics and its effect on cross-sectional temperature fields and local heat transfer coefficients have been previously studied by means of CFD [38]. It implies that hot elements of fluid that may be located at the top wall at the entrance, or cold ones located at the bottom wall, can be detected at different heights all along the channel. In Table 4, it also appears that the three average temperatures measured at the first position (i.e. x = 0.034 m for *Re* = 503, x = 0.045 m for *Re* = 695) show less relative difference, around 2%, than in the following positions. This may be due to

entrance effects, where singularities at the inlet can favor cross-sectional mixing in the zone investigated (between 1 mm and 3 mm height, for a total channel depth of 4 mm). Then, the relative difference increases at the second position (around 10%), due to both the contribution of Dean vortices and thermal diffusive effects from the walls to the middle of the channel. Finally, the relative difference decreases as the temperature difference between the hot fluid and the cold fluid decreases (around 5% at the third position).

Table 4. Temperature measurements in the zigzag channel with heat transfer (uncertainty on $T_{p,PLIF}$ are determined with Eq. (10), uncertainty on T_{in} and T_{out} considers temperature variation between the 3 experiments and thermocouple accuracy)

Re	*x*	$T_{p,PLIF}$ (°C)			$T_{p,in}$	$T_{p,out}$	$T_{u,in}$	$T_{u,out}$
	(m)	High plane	Medium plane	Low plane	(°C)	(°C)	(°C)	(°C)
503	0.034	52.2±1.3	53.1±1.3	51.8±1.3	56.9±0.4	28.3±0.4	18.9±0.5	19.6±0.5
	0.069	55.2±1.4	50.1±1.2	51.1±1.3	56.9±0.4	28.5±0.4	19.5±0.4	20.2±0.4
	0.138	49.4±1.2	46.6±1.1	47.0±1.1	56.9±0.5	29.6±0.4	21.1±0.4	21.8±0.5
695	0.045	53.4±1.4	53.6±1.4	52.6±1.3	57.5±0.4	35.6±0.5	27.0±0.5	27.7±0.6
	0.092	54.5±1.4	51.4±1.3	49.5±1.2	57.5±0.4	33.3±0.5	23.6±0.5	24.4±0.5
	0.175	47.4±1.1	47.2±1.1	45.0±1.0	57.4±0.4	32.1±0.8	22.0±0.8	22.7±0.8

To conclude, the general trends observed tend to validate the consistency of the local thermometry method based on two-color/two-dye PLIF technique. In order to evaluate the reliability of the PLIF thermometry method, a heat transfer model is introduced which can estimate the mean temperature profile of the process fluid to enable the comparison with the measurements.

6.3 Comparison between temperatures measured by PLIF technique and calculated by heat transfer model

A 1D heat transfer model is used to calculate the temperature of the process fluid in the zigzag channel as a function of the length in the channel (x-position) and the inlet and outlet temperature of both fluids. It can be expressed as follows:

$$u_p \rho_p c_{P,p} \frac{dT_{p,x}}{dx} = \frac{U dA (T_{u,y} - T_{p,x}) - U_l dA (T_{p,x} - T_{air})}{dV_p} \quad (11)$$

where u_p, ρ_p and $c_{P,p}$ are the velocity, density and specific heat capacity of the process fluid respectively. $T_{p,x}$ is the mean temperature at length x of the process fluid and $T_{u,y}$ is the mean temperature at length y of the utility fluid (Fig. 11). As the total channel lengths in the two plates are different, corresponding lengths are related as follows:

$$y = \frac{x L_u}{L_p} \quad (12)$$

where $L_p$and L_u are the total lengths of the process channel and the utility channel.

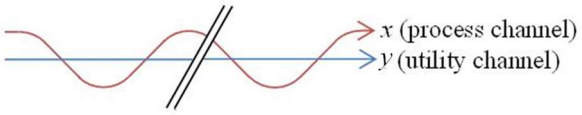

Fig. 11. Illustration of the axial coordinates in the process and utility channels

T_{air} is the temperature of air and it is taken at 20 °C. dA and dV_p are the elementary heat transfer area and the elementary volume of process fluid corresponding to the channel length element dx. U is the overall heat transfer coefficient of the prototype and U_l is the overall heat transfer coefficient relative to the heat loss, which is calculated from a prior experiment with no utility fluid:

$$U_l = \frac{q_l}{A\Delta T_{ml,l}} = \frac{\dot{m}_p C_{P,p} \Delta T_{p,l}}{A\Delta T_{ml,l}} \tag{13}$$

where q_l is the global heat loss. A is the total heat exchange area, equals to the zigzag channel width, 0.004 m, multiplied by its developed length, 0.75 m. $\Delta T_{ml,l}$ is expressed as follows:

$$\Delta T_{ml,l} = \frac{(T_{p,in,l} - T_{air}) - (T_{p,out,l} - T_{air})}{\ln\left(\frac{T_{p,in,l} - T_{air}}{T_{p,out,l} - T_{air}}\right)} \tag{14}$$

where $T_{p,in,l}$ and $T_{p,out,l}$ are the inlet and the outlet temperatures measured during the heat loss experiment.

For the utility fluid, there is a similar equation to calculate the temperature:

$$u_u \rho_u c_{P,u} \frac{dT_{u,y}}{ds} = \frac{U dA}{dV_u}\left(T_{p,x} - T_{u,y}\right) \tag{15}$$

where u_u, ρ_u and $c_{P,u}$ are the velocity, density and specific heat capacity of the utility fluid respectively. dV_u is the elementary volume of utility fluid corresponding to the channel length element dy. The thermal loss in the utility side is neglected since its temperature is close to room temperature and the temperature difference between inlet and outlet is less than 1°C during the experiment. Finally, the overall heat exchange coefficient is calculated from the inlet and outlet temperatures measured by the thermocouples:

$$U = \frac{q}{A\Delta T_{ml}} = \frac{\dot{m}_p C_{P,p} \Delta T_p}{A\Delta T_{ml}} \tag{16}$$

$$\Delta T_{ml} = \frac{(T_{p,in} - T_{u,in}) - (T_{p,out} - T_{u,out})}{\ln\left(\frac{T_{p,in} - T_{u,in}}{T_{p,out} - T_{p,out}}\right)} \tag{17}$$

The temperatures of the process fluid and the utility fluid can be deduced from Eq. (11) and Eq. (15). At $x = 0$ and $y = 0$, the average experimental inlet temperatures of the two fluids given in Table 4 are set.

The temperature profiles calculated with the heat transfer model at $Re = 503$ and $Re = 695$ are shown in Fig. 12 and Fig. 13 respectively. The profiles in each figure is calculated from the mean values of the inlet temperature, the outlet temperatures and the overall heat transfer coefficient deduced from Eq. (16) and Eq. (17) obtained for the three experiments carried out at a same channel length (corresponding to the three different heights investigated). The profiles can be compared with the experimental measurements, where the crosses correspond to the mean inlet and outlet temperatures measured by the

thermocouples. The full dots correspond to the average temperature over the observed field measured by the PLIF technique at different length and height in the channel. First, it can be seen that the outlet temperatures measured and calculated by the model are in very good agreement, showing the consistency of the model. Secondly, the maximal difference between the measured temperatures in medium planes of the channel (2 mm depth) and the calculated ones is 2.1°C, i.e. 4% of relative difference, which is satisfying as the model gives an average of the temperature over the cross-section all along the channel, calculated with a constant overall heat transfer coefficient. The high plane appears to be the hottest in all the experiments as expected since it is the furthest from the cold fluid.

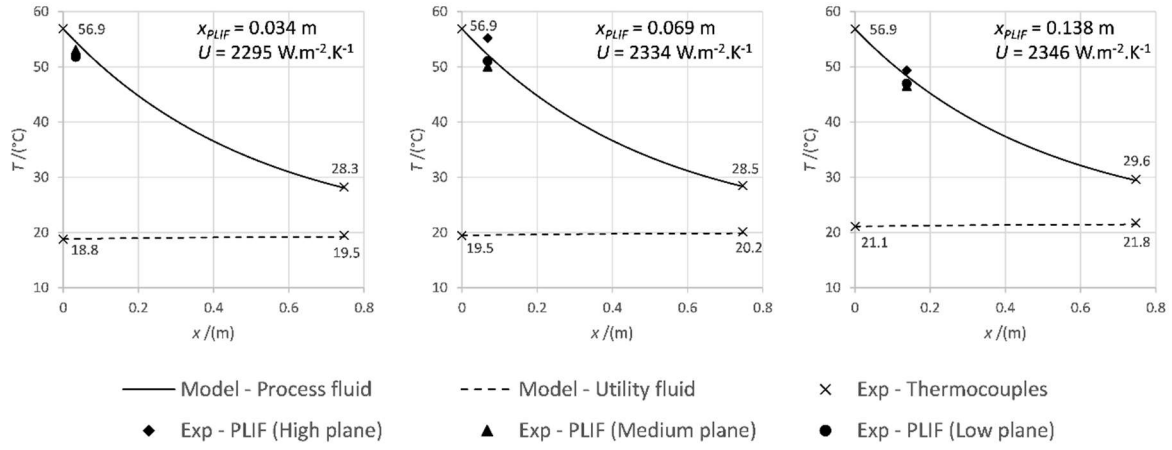

Fig. 12. Comparison between the temperature profiles obtained by heat transfer modelling and experimental measurements by PLIF thermometry at different length in the channel for Re = 503 (U_l = 169 W.m^{-2}.K^{-1} ; T_{air} = 20 °C)

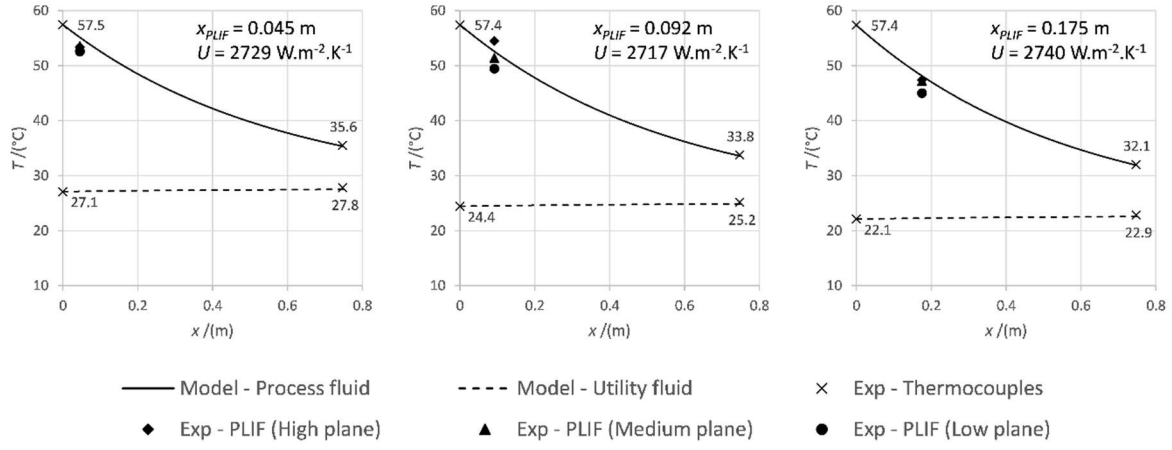

Fig. 13. Comparison between the temperature profiles obtained by heat transfer modelling and experimental measurements by PLIF thermometry at different length in the channel for Re = 695 (U_l = 171 W.m^{-2}.K^{-1} ; T_{air} = 20 °C)

In consideration with the desired applications in compacts heat exchangers reactors, the temperature fields obtained are very consistent and satisfactorily accurate to be able to estimate local heat transfer coefficient without disturbing the fluid flow, despite the variations in the optical paths particularly due to the zigzag geometry. Moreover, the observed resolution in space and time enables to detect temperature heterogeneities and notably significant hot or cold spot that can be dramatic for the implementation of chemical reactions.

7. Conclusion

The technique of temperature measurement based on planar laser-induced fluorescence with two-color/two-dye is developed and applied to measure local temperatures during heat transfer in a square millimetric zigzag channel of 4 mm depth. This method is highly documented in literature but has been originally used in this work in a highly confined liquid flow, with a complex channel geometry. First, a method calibration is developed and is checked analyzing temperature fields obtained while the fluid temperature is constant. The sensitivity of the implemented method is good, equals to $3.3\%.C^{-1}$ in terms of fluorescence signal ratio. Global uncertainty of the measurement is estimated to be lower than 3% in the temperature range of 17-60°C. Then, the temperature fields at different heights and at different locations in the zigzag channels are investigated during heat transfer. The average temperatures are compared with that obtained with a 1D heat transfer model and show a good agreement. The method provides images with a satisfying resolution in space and time to be able to highlight temperature heterogeneities and instabilities. Therefore, it can be concluded that this non-intrusive thermometry technique presents a good potential for local instantaneous temperature measurements in millimetric channels and in compact devices in general. In addition to this study, it could then be interesting to compare experimental temperature fields obtained by PLIF technique with CFD results.

Acknowledgments

This work was performed using equipments from the Fédération de Recherche Fermat, FR 3089.

Nomenclature

a	calibration coefficient (-)
A	heat transfer area (m^2)
b	calibration coefficient (-)
C	molar concentration of the dye ($mol.L^{-1}$)
C_p	specific heat capacity ($J.kg^{-1}.K^{-1}$)
d_h	hydraulic diameter (m)
e	thickness of aluminum plate (m)
F	fluorescence signal (Absorbance Unit A.U.)
k	thermal conductivity ($W.m^{-1}.K^{-1}$)

L channel length (m)

L_s straight section length (m)

I_0 laser intensity ($W.m^{-2}$)

I_{sat} saturation intensity of the fluorescent dye ($W.m^{-2}$)

R fluorescence ratio (-)

R_c radius of curvature (m)

Re Reynolds number (-)

R_0 fluorescence ratio at reference temperature (-)

q heat flux (W)

s sensitivity coefficient ($°C^{-1}$)

T temperature (K)

T_0 reference temperature (K)

u velocity ($m.s^{-1}$)

U global heat transfer coefficient ($W.m^{-2}.K^{-1}$)

V volume (m^3)

x axial coordinate in the process channel (m)

y axial coordinate in the utility channel (m)

Greek symbols

λ wavelength (nm)

η transmission efficiency of the fluorescence light (-)

Ω solid angle of the collection (rad)

ε_0 molar absorptivity of the fluorescent molecules (A.U. $m^2.mol^{-1}$)

ϕ fluorescence quantum yield (-)

θ angle between two straight sections (°)

ρ density ($kg.m^{-3}$)

ΔX uncertainty on variable X (unit of X)

Subscripts

FL fluorescein

in	inlet
l	heat loss
m	mean value
out	outlet
p	process fluid
SRB	sulforhodamine B
u	utility fluid

References

[1] Z. Anxionnaz, M. Cabassud, C. Gourdon, P. Tochon, Heat exchanger/reactors (HEX reactors): Concepts, technologies: State-of-the-art, Chem. Eng. Process. Process Intensif. 47 (2008) 2029–2050. https://doi.org/10.1016/j.cep.2008.06.012.

[2] Q. Li, G. Flamant, X. Yuan, P. Neveu, L. Luo, Compact heat exchangers: A review and future applications for a new generation of high temperature solar receivers, Renew. Sustain. Energy Rev. 15 (2011) 4855–4875. https://doi.org/10.1016/j.rser.2011.07.066.

[3] R.J. Adrian, Twenty years of particle image velocimetry, Exp. Fluids. 39 (2005) 159–169. https://doi.org/10.1007/s00348-005-0991-7.

[4] J.G. Santiago, S.T. Wereley, C.D. Meinhart, D.J. Beebe, R.J. Adrian, A particle image velocimetry system for microfluidics, Exp. Fluids. 25 (1998) 316–319.

[5] S. Elgue, A. Conté, C. Gourdon, Y. Bastard, Direct fluorination of 1,3-dicarbonyl compound in a continuous flow reactor at industrial scale, Chem. Today. 30 (2012).

[6] N. Di Miceli Raimondi, N. Olivier-Maget, N. Gabas, M. Cabassud, C. Gourdon, Safety enhancement by transposition of the nitration of toluene from semi-batch reactor to continuous intensified heat exchanger reactor, Chem. Eng. Res. Des. 94 (2015) 182–193. https://doi.org/10.1016/j.cherd.2014.07.029.

[7] L. Wang, F. Liu, Forced convection in slightly curved microchannels, Int. J. Heat Mass Transf. 50 (2007) 881–896. https://doi.org/10.1016/j.ijheatmasstransfer.2006.08.016.

[8] Y. Sui, C.J. Teo, P.S. Lee, Y.T. Chew, C. Shu, Fluid flow and heat transfer in wavy microchannels, Int. J. Heat Mass Transf. 53 (2010) 2760–2772. https://doi.org/10.1016/j.ijheatmasstransfer.2010.02.022.

[9] Z. Zheng, D.F. Fletcher, B.S. Haynes, Chaotic advection in steady laminar heat transfer simulations: Periodic zigzag channels with square cross-sections, Int. J. Heat Mass Transf. 57 (2013) 274–284. https://doi.org/10.1016/j.ijheatmasstransfer.2012.10.029.

[10] H. Shi, N. Di Miceli Raimondi, D.F. Fletcher, M. Cabassud, C. Gourdon, Numerical study of heat transfer in square millimetric zigzag channels in the laminar flow regime, Chem. Eng. Process. - Process Intensif. 144 (2019) 107624. https://doi.org/10.1016/j.cep.2019.107624.

[11] D. Dabiri, M. Gharib, Digital particle image thermometry: the method and implementation, Exp. Fluids. 11 (1991) 77–86.

[12] D.R. Sabatino, T.J. Praisner, C.R. Smith, A high-accuracy calibration technique for thermochromic liquid crystal temperature measurements, Exp. Fluids. 28 (2000) 497–505. https://doi.org/10.1007/s003480050411.

[13] C. Pradere, M. Joanicot, J.-C. Batsale, J. Toutain, C. Gourdon, Processing of temperature field in chemical microreactors with infrared thermography, Quant. InfraRed Thermogr. J. 3 (2006) 117–135. https://doi.org/10.3166/qirt.3.117-135.
[14] D. Ghiasy, K.V.K. Boodhoo, M.T. Tham, Thermographic analysis of thin liquid films on a rotating disc: Approach and challenges, Appl. Therm. Eng. 44 (2012) 39–49. https://doi.org/10.1016/j.applthermaleng.2012.04.006.
[15] J. Haber, B. Jiang, T. Maeder, N. Borhani, J. Thome, A. Renken, L. Kiwi-Minsker, Intensification of highly exothermic fast reaction by multi-injection microstructured reactor, Chem. Eng. Process. Process Intensif. 84 (2014) 14–23. https://doi.org/10.1016/j.cep.2014.02.007.
[16] J.S. Zhang, C.Y. Zhang, G.T. Liu, G.S. Luo, Measuring enthalpy of fast exothermal reaction with infrared thermography in a microreactor, Chem. Eng. J. 295 (2016) 384–390. https://doi.org/10.1016/j.cej.2016.01.100.
[17] C. Zhang, J. Zhang, G. Luo, Kinetics determination of fast exothermic reactions with infrared thermography in a microreactor, J. Flow Chem. 10 (2020) 219–226. https://doi.org/10.1007/s41981-019-00071-8.
[18] T. Nakajima, M. Utsunomiya, Y. Ikeda, Simultaneous Measurement of Velocity and Temperature of Water Using LDV and Fluorescence Technique, in: R.J. Adrian, D.F.G. Durão, F. Durst, M. Maeda, J. Whitelaw (Eds.), Appl. Laser Tech. Fluid Mech., Springer Berlin Heidelberg, Berlin, Heidelberg, 1991: pp. 34–53. https://doi.org/10.1007/978-3-642-61254-1_3.
[19] F. Lemoine, Y. Antoine, M. Wolff, M. Lebouche, Simultaneous temperature and 2D velocity measurements in a turbulent heated jet using combined laser-induced fluorescence and LDA, Exp. Fluids. 26 (1999) 315–323. https://doi.org/10.1007/s003480050294.
[20] J. Sakakibara, K. Hishida, M. Maeda, Measurements of thermally stratified pipe flow using image-processing techniques, Exp. Fluids. 16 (1993) 82–96. https://doi.org/10.1007/BF00944910.
[21] M.C.J. Coolen, R.N. Kieft, C.C.M. Rindt, A.A. van Steenhoven, Application of 2-D LIF temperature measurements in water using a Nd : YAG laser, Exp. Fluids. 27 (1999) 420–426. https://doi.org/10.1007/s003480050367.
[22] M. Bruchhausen, F. Guillard, F. Lemoine, Instantaneous measurement of two-dimensional temperature distributions by means of two-color planar laser induced fluorescence (PLIF), Exp. Fluids. 38 (2005) 123–131. https://doi.org/10.1007/s00348-004-0911-2.
[23] G. Castanet, A. Labergue, F. Lemoine, International Journal of Thermal Sciences Internal temperature distributions of interacting and vaporizing droplets, Int. J. Therm. Sci. 50 (2011) 1181–1190. https://doi.org/10.1016/j.ijthermalsci.2011.02.001.
[24] J. Sakakibara, R.J. Adrian, Whole field measurement of temperature in water using two-color laser induced fluorescence, Exp. Fluids. 26 (1999) 7–15. https://doi.org/10.1007/s003480050260.
[25] J. Sakakibara, R.J. Adrian, Measurement of temperature field of a Rayleigh-Bénard convection using two-color laser-induced fluorescence, Exp. Fluids. 37 (2004) 331–340. https://doi.org/10.1007/s00348-004-0821-3.
[26] H.J. Kim, K.D. Kihm, J.S. Allen, Examination of ratiometric laser induced fluorescence thermometry for microscale spatial measurement resolution, Int. J. Heat Mass Transf. 46 (2003) 3967–3974. https://doi.org/10.1016/S0017-9310(03)00243-6.
[27] W. Chaze, O. Caballina, G. Castanet, F. Lemoine, Spatially and temporally resolved measurements of the temperature inside droplets impinging on a hot solid surface, Exp. Fluids. 58 (2017) 1–16. https://doi.org/10.1007/s00348-017-2375-1.

[28] J.A. Sutton, B.T. Fisher, J.W. Fleming, A laser-induced fluorescence measurement for aqueous fluid flows with improved temperature sensitivity, Exp. Fluids. 45 (2008) 869–881. https://doi.org/10.1007/s00348-008-0506-4.
[29] M.B. Shafii, C.L. Lum, M.M. Koochesfahani, In situ LIF temperature measurements in aqueous ammonium chloride solution during uni-directional solidification, Exp. Fluids. 48 (2010) 651–662. https://doi.org/10.1007/s00348-009-0758-7.
[30] O. Filevich, R. Etchenique, 1D and 2D Temperature Imaging with a Fluorescent Ruthenium Complex, Anal. Chem. 78 (2006) 7499–7503. https://doi.org/10.1021/ac061382f.
[31] S.A. Pfeiffer, S. Nagl, Microfluidic platforms employing integrated fluorescent or luminescent chemical sensors: a review of methods, scope and applications, Methods Appl. Fluoresc. 3 (2015) 034003. https://doi.org/10.1088/2050-6120/3/3/034003.
[32] M.A. Bennet, P.R. Richardson, J. Arlt, A. McCarthy, G.S. Buller, A.C. Jones, Optically trapped microsensors for microfluidic temperature measurement by fluorescence lifetime imaging microscopy, Lab. Chip. 11 (2011) 3821–3828. https://doi.org/10.1039/C1LC20391F.
[33] W. Chaze, O. Caballina, G. Castanet, F. Lemoine, The saturation of the fluorescence and its consequences for laser-induced fluorescence thermometry in liquid flows, Exp. Fluids. 57 (2016) 58. https://doi.org/10.1007/s00348-016-2142-8.
[34] J. Coppeta, C. Rogers, Dual emission laser induced fluorescence for direct planar scalar behavior measurements, Exp. Fluids. 25 (1998) 1–15. https://doi.org/10.1007/s003480050202.
[35] M.M. Martin, L. Lindqvist, The pH dependence of fluorescein fluorescence, J. Lumin. 10 (1975) 381–390.
[36] N. Klonis, W.H. Sawyer, Spectral properties of the prototropic forms of fluorescein in aqueous solution, J. Fluoresc. 6 (1996) 147–157. https://doi.org/10.1007/BF00732054.
[37] L. Despènes, S. Elgue, C. Gourdon, M. Cabassud, Impact of the material on the thermal behaviour of heat exchangers-reactors, Chem. Eng. Process. Process Intensif. 52 (2012) 102–111. https://doi.org/10.1016/j.cep.2011.11.005.
[38] H. Shi, N. Di Miceli Raimondi, D.F. Fletcher, M. Cabassud, C. Gourdon, Numerical study of heat transfer in square millimetric zigzag channels in the laminar flow regime, Chem. Eng. Process. - Process Intensif. 144 (2019) 107624. https://doi.org/10.1016/j.cep.2019.107624.
[39] R.J. Moffat, Describing the uncertainties in experimental results, Exp. Therm. Fluid Sci. 1 (1988) 3–17. https://doi.org/10.1016/0894-1777(88)90043-X.